

Evidence for $D^0 - \bar{D}^0$ Mixing Using the CDF II Detector

T. Aaltonen,²³ J. Adelman,¹³ T. Akimoto,⁵⁴ M.G. Albrow,¹⁷ B. Álvarez González,¹¹ S. Amerio,⁴² D. Amidei,³⁴ A. Anastassov,⁵¹ A. Annovi,¹⁹ J. Antos,¹⁴ M. Aoki,²⁴ G. Apollinari,¹⁷ A. Apresyan,⁴⁷ T. Arisawa,⁵⁶ A. Artikov,¹⁵ W. Ashmanskas,¹⁷ A. Attal,³ A. Aurisano,⁵² F. Azfar,⁴¹ P. Azzi-Bacchetta,⁴² P. Azzurri,⁴⁵ N. Bacchetta,⁴² W. Badgett,¹⁷ A. Barbaro-Galtieri,²⁸ V.E. Barnes,⁴⁷ B.A. Barnett,²⁵ S. Baroiant,⁷ V. Bartsch,³⁰ G. Bauer,³² P.-H. Beauchemin,³³ F. Bedeschi,⁴⁵ P. Bednar,¹⁴ S. Behari,²⁵ G. Bellettini,⁴⁵ J. Bellinger,⁵⁸ A. Belloni,²² D. Benjamin,¹⁶ A. Beretvas,¹⁷ J. Beringer,²⁸ T. Berry,²⁹ A. Bhatti,⁴⁹ M. Binkley,¹⁷ D. Bisello,⁴² I. Bizjak,³⁰ R.E. Blair,² C. Blocker,⁶ B. Blumenfeld,²⁵ A. Bocci,¹⁶ A. Bodek,⁴⁸ V. Boisvert,⁴⁸ G. Bolla,⁴⁷ A. Bolshov,³² D. Bortoletto,⁴⁷ J. Boudreau,⁴⁶ A. Boveia,¹⁰ B. Brau,¹⁰ A. Bridgeman,²⁴ L. Brigliadori,⁵ C. Bromberg,³⁵ E. Brubaker,¹³ J. Budagov,¹⁵ H.S. Budd,⁴⁸ S. Budd,²⁴ K. Burkett,¹⁷ G. Busetto,⁴² P. Bussey,²¹ A. Buzatu,³³ K. L. Byrum,² S. Cabrera^r,¹⁶ M. Campanelli,³⁵ M. Campbell,³⁴ F. Canelli,¹⁷ A. Canepa,⁴⁴ D. Carlsmith,⁵⁸ R. Carosi,⁴⁵ S. Carrillo^l,¹⁸ S. Carron,³³ B. Casal,¹¹ M. Casarsa,¹⁷ A. Castro,⁵ P. Catastini,⁴⁵ D. Cauz,⁵³ M. Cavalli-Sforza,³ A. Cerri,²⁸ L. Cerrito^p,³⁰ S.H. Chang,²⁷ Y.C. Chen,¹ M. Chertok,⁷ G. Chiarelli,⁴⁵ G. Chlachidze,¹⁷ F. Chlebana,¹⁷ K. Cho,²⁷ D. Chokheli,¹⁵ J.P. Chou,²² G. Choudalakis,³² S.H. Chuang,⁵¹ K. Chung,¹² W.H. Chung,⁵⁸ Y.S. Chung,⁴⁸ C.I. Ciobanu,²⁴ M.A. Ciocci,⁴⁵ A. Clark,²⁰ D. Clark,⁶ G. Compostella,⁴² M.E. Convery,¹⁷ J. Conway,⁷ B. Cooper,³⁰ K. Copic,³⁴ M. Cordelli,¹⁹ G. Cortiana,⁴² F. Crescioli,⁴⁵ C. Cuenca Almenar^r,⁷ J. Cuevas^o,¹¹ R. Culbertson,¹⁷ J.C. Cully,³⁴ D. Dagenhart,¹⁷ M. Datta,¹⁷ T. Davies,²¹ P. de Barbaro,⁴⁸ S. De Cecco,⁵⁰ A. Deisher,²⁸ G. De Lentdecker^d,⁴⁸ G. De Lorenzo,³ M. Dell'Orso,⁴⁵ L. Demortier,⁴⁹ J. Deng,¹⁶ M. Deninno,⁵ D. De Pedis,⁵⁰ P.F. Derwent,¹⁷ G.P. Di Giovanni,⁴³ C. Dionisi,⁵⁰ B. Di Ruzza,⁵³ J.R. Dittmann,⁴ M. D'Onofrio,³ S. Donati,⁴⁵ P. Dong,⁸ J. Donini,⁴² T. Dorigo,⁴² S. Dube,⁵¹ J. Efron,³⁸ R. Erbacher,⁷ D. Errede,²⁴ S. Errede,²⁴ R. Eusebi,¹⁷ H.C. Fang,²⁸ S. Farrington,²⁹ W.T. Fedorko,¹³ R.G. Feild,⁵⁹ M. Feindt,²⁶ J.P. Fernandez,³¹ C. Ferrazza,⁴⁵ R. Field,¹⁸ G. Flanagan,⁴⁷ R. Forrest,⁷ S. Forrester,⁷ M. Franklin,²² J.C. Freeman,²⁸ I. Furic,¹⁸ M. Gallinaro,⁴⁹ J. Galyardt,¹² F. Garberson,¹⁰ J.E. Garcia,⁴⁵ A.F. Garfinkel,⁴⁷ H. Gerberich,²⁴ D. Gerdes,³⁴ S. Giagu,⁵⁰ V. Giakoumopolou^a,⁴⁵ P. Giannetti,⁴⁵ K. Gibson,⁴⁶ J.L. Gimmell,⁴⁸ C.M. Ginsburg,¹⁷ N. Giokaris^a,¹⁵ M. Giordani,⁵³ P. Giromini,¹⁹ M. Giunta,⁴⁵ V. Glagolev,¹⁵ D. Glenzinski,¹⁷ M. Gold,³⁶ N. Goldschmidt,¹⁸ A. Golossanov,¹⁷ G. Gomez,¹¹ G. Gomez-Ceballos,³² M. Goncharov,⁵² O. González,³¹ I. Gorelov,³⁶ A.T. Goshaw,¹⁶ K. Goulianos,⁴⁹ A. Gresele,⁴² S. Grinstein,²² C. Grosso-Pilcher,¹³ R.C. Group,¹⁷ U. Grundler,²⁴ J. Guimaraes da Costa,²² Z. Gunay-Unalan,³⁵ C. Haber,²⁸ K. Hahn,³² S.R. Hahn,¹⁷ E. Halkiadakis,⁵¹ A. Hamilton,²⁰ B.-Y. Han,⁴⁸ J.Y. Han,⁴⁸ R. Handler,⁵⁸ F. Happacher,¹⁹ K. Hara,⁵⁴ D. Hare,⁵¹ M. Hare,⁵⁵ S. Harper,⁴¹ R.F. Harr,⁵⁷ R.M. Harris,¹⁷ M. Hartz,⁴⁶ K. Hatakeyama,⁴⁹ J. Hauser,⁸ C. Hays,⁴¹ M. Heck,²⁶ A. Heijboer,⁴⁴ B. Heinemann,²⁸ J. Heinrich,⁴⁴ C. Henderson,³² M. Herndon,⁵⁸ J. Heuser,²⁶ S. Hewamanage,⁴ D. Hidas,¹⁶ C.S. Hill^c,¹⁰ D. Hirschbuehl,²⁶ A. Hocker,¹⁷ S. Hou,¹ M. Houlden,²⁹ S.-C. Hsu,⁹ B.T. Huffman,⁴¹ R.E. Hughes,³⁸ U. Husemann,⁵⁹ J. Huston,³⁵ J. Incandela,¹⁰ G. Introzzi,⁴⁵ M. Iori,⁵⁰ A. Ivanov,⁷ B. Iyutin,³² E. James,¹⁷ B. Jayatilaka,¹⁶ D. Jeans,⁵⁰ E.J. Jeon,²⁷ S. Jindariani,¹⁸ W. Johnson,⁷ M. Jones,⁴⁷ K.K. Joo,²⁷ S.Y. Jun,¹² J.E. Jung,²⁷ T.R. Junk,²⁴ T. Kamon,⁵² D. Kar,¹⁸ P.E. Karchin,⁵⁷ Y. Kato,⁴⁰ R. Kephart,¹⁷ U. Kerzel,²⁶ V. Khotilovich,⁵² B. Kilminster,³⁸ D.H. Kim,²⁷ H.S. Kim,²⁷ J.E. Kim,²⁷ M.J. Kim,¹⁷ S.B. Kim,²⁷ S.H. Kim,⁵⁴ Y.K. Kim,¹³ N. Kimura,⁵⁴ L. Kirsch,⁶ S. Klimenko,¹⁸ M. Klute,³² B. Knuteson,³² B.R. Ko,¹⁶ S.A. Koay,¹⁰ K. Kondo,⁵⁶ D.J. Kong,²⁷ J. Konigsberg,¹⁸ A. Korytov,¹⁸ A.V. Kotwal,¹⁶ J. Kraus,²⁴ M. Kreps,²⁶ J. Kroll,⁴⁴ N. Krumnack,⁴ M. Kruse,¹⁶ V. Krutelyov,¹⁰ T. Kubo,⁵⁴ S. E. Kuhlmann,² T. Kuhr,²⁶ N.P. Kulkarni,⁵⁷ Y. Kusakabe,⁵⁶ S. Kwang,¹³ A.T. Laasanen,⁴⁷ S. Lai,³³ S. Lami,⁴⁵ S. Lammel,¹⁷ M. Lancaster,³⁰ R.L. Lander,⁷ K. Lannon,³⁸ A. Lath,⁵¹ G. Latino,⁴⁵ I. Lazzizzera,⁴² T. LeCompte,² J. Lee,⁴⁸ J. Lee,²⁷ Y.J. Lee,²⁷ S.W. Lee^q,⁵² R. Lefèvre,²⁰ N. Leonardo,³² S. Leone,⁴⁵ S. Levy,¹³ J.D. Lewis,¹⁷ C. Lin,⁵⁹ C.S. Lin,²⁸ J. Linacre,⁴¹ M. Lindgren,¹⁷ E. Lipeles,⁹ A. Lister,⁷ D.O. Litvintsev,¹⁷ T. Liu,¹⁷ N.S. Lockyer,⁴⁴ A. Loginov,⁵⁹ M. Loretì,⁴² L. Lovas,¹⁴ R.-S. Lu,¹ D. Lucchesi,⁴² J. Lueck,²⁶ C. Luci,⁵⁰ P. Lujan,²⁸ P. Lukens,¹⁷ G. Lungu,¹⁸ L. Lyons,⁴¹ J. Lys,²⁸ R. Lysak,¹⁴ E. Lytken,⁴⁷ P. Mack,²⁶ D. MacQueen,³³ R. Madrak,¹⁷ K. Maeshima,¹⁷ K. Makhoul,³² T. Maki,²³ P. Maksimovic,²⁵ S. Malde,⁴¹ S. Malik,³⁰ G. Manca,²⁹ A. Manousakis^a,¹⁵ F. Margaroli,⁴⁷ C. Marino,²⁶ C.P. Marino,²⁴ A. Martin,⁵⁹ M. Martin,²⁵ V. Martin^j,²¹ M. Martínez,³ R. Martínez-Ballarín,³¹ T. Maruyama,⁵⁴ P. Mastrandrea,⁵⁰ T. Masubuchi,⁵⁴ M.E. Mattson,⁵⁷ P. Mazzanti,⁵ K.S. McFarland,⁴⁸ P. McIntyre,⁵² R. McNultyⁱ,²⁹ A. Mehta,²⁹ P. Mehtala,²³ S. Menzemer^k,¹¹ A. Menzione,⁴⁵ P. Merkel,⁴⁷ C. Mesropian,⁴⁹ A. Messina,³⁵ T. Miao,¹⁷ N. Miladinovic,⁶ J. Miles,³² R. Miller,³⁵ C. Mills,²² M. Milnik,²⁶ A. Mitra,¹ G. Mitselmakher,¹⁸ H. Miyake,⁵⁴ S. Moed,²² N. Moggi,⁵ C.S. Moon,²⁷ R. Moore,¹⁷ M. Morello,⁴⁵ P. Movilla Fernandez,²⁸ J. Müllenstädt,²⁸

A. Mukherjee,¹⁷ Th. Muller,²⁶ R. Mumford,²⁵ P. Murat,¹⁷ M. Mussini,⁵ J. Nachtman,¹⁷ Y. Nagai,⁵⁴ A. Nagano,⁵⁴ J. Naganoma,⁵⁶ K. Nakamura,⁵⁴ I. Nakano,³⁹ A. Napier,⁵⁵ V. Necula,¹⁶ C. Neu,⁴⁴ M.S. Neubauer,²⁴ J. Nielsen,^{f,28} L. Nodulman,² M. Norman,⁹ O. Norniella,²⁴ E. Nurse,³⁰ S.H. Oh,¹⁶ Y.D. Oh,²⁷ I. Oksuzian,¹⁸ T. Okusawa,⁴⁰ R. Oldeman,²⁹ R. Orava,²³ K. Osterberg,²³ S. Pagan Griso,⁴² C. Pagliarone,⁴⁵ E. Palencia,¹⁷ V. Papadimitriou,¹⁷ A. Papaikonomou,²⁶ A.A. Paramonov,¹³ B. Parks,³⁸ S. Pashapour,³³ J. Patrick,¹⁷ G. Pauletta,⁵³ M. Paulini,¹² C. Paus,³² D.E. Pellett,⁷ A. Penzo,⁵³ T.J. Phillips,¹⁶ G. Piacentino,⁴⁵ J. Piedra,⁴³ L. Pinera,¹⁸ K. Pitts,²⁴ C. Plager,⁸ L. Pondrom,⁵⁸ X. Portell,³ O. Poukhov,¹⁵ N. Pounder,⁴¹ F. Prakoshyn,¹⁵ A. Pronko,¹⁷ J. Proudfoot,² F. Ptohos,^{h,17} G. Punzi,⁴⁵ J. Pursley,⁵⁸ J. Rademacker,^{c,41} A. Rahaman,⁴⁶ V. Ramakrishnan,⁵⁸ N. Ranjan,⁴⁷ I. Redondo,³¹ B. Reisert,¹⁷ V. Rekovic,³⁶ P. Renton,⁴¹ M. Rescigno,⁵⁰ S. Richter,²⁶ F. Rimondi,⁵ L. Ristori,⁴⁵ A. Robson,²¹ T. Rodrigo,¹¹ E. Rogers,²⁴ S. Rolli,⁵⁵ R. Roser,¹⁷ M. Rossi,⁵³ R. Rossin,¹⁰ P. Roy,³³ A. Ruiz,¹¹ J. Russ,¹² V. Rusu,¹⁷ H. Saarikko,²³ A. Safonov,⁵² W.K. Sakumoto,⁴⁸ G. Salamanna,⁵⁰ O. Saltó,³ L. Santi,⁵³ S. Sarkar,⁵⁰ L. Sartori,⁴⁵ K. Sato,¹⁷ A. Savoy-Navarro,⁴³ T. Scheidle,²⁶ P. Schlabach,¹⁷ E.E. Schmidt,¹⁷ M.A. Schmidt,¹³ M.P. Schmidt,⁵⁹ M. Schmitt,³⁷ T. Schwarz,⁷ L. Scodellaro,¹¹ A.L. Scott,¹⁰ A. Scribano,⁴⁵ F. Scuri,⁴⁵ A. Sedov,⁴⁷ S. Seidel,³⁶ Y. Seiya,⁴⁰ A. Semenov,¹⁵ L. Sexton-Kennedy,¹⁷ A. Sfyria,²⁰ S.Z. Shalhout,⁵⁷ M.D. Shapiro,²⁸ T. Shears,²⁹ P.F. Shepard,⁴⁶ D. Sherman,²² M. Shimojima,^{n,54} M. Shochet,¹³ Y. Shon,⁵⁸ I. Shreyber,²⁰ A. Sidoti,⁴⁵ P. Sinervo,³³ A. Sisakyan,¹⁵ A.J. Slaughter,¹⁷ J. Slaunwhite,³⁸ K. Sliwa,⁵⁵ J.R. Smith,⁷ F.D. Snider,¹⁷ R. Snihur,³³ M. Soderberg,³⁴ A. Soha,⁷ S. Somalwar,⁵¹ V. Sorin,³⁵ J. Spalding,¹⁷ F. Spinella,⁴⁵ T. Spreitzer,³³ P. Squillacioti,⁴⁵ M. Stanitzki,⁵⁹ R. St. Denis,²¹ B. Stelzer,⁸ O. Stelzer-Chilton,⁴¹ D. Stentz,³⁷ J. Strogas,³⁶ D. Stuart,¹⁰ J.S. Suh,²⁷ A. Sukhanov,¹⁸ H. Sun,⁵⁵ I. Suslov,¹⁵ T. Suzuki,⁵⁴ A. Taffard,^{e,24} R. Takashima,³⁹ Y. Takeuchi,⁵⁴ R. Tanaka,³⁹ M. Tecchio,³⁴ P.K. Teng,¹ K. Terashi,⁴⁹ J. Thom,^{g,17} A.S. Thompson,²¹ G.A. Thompson,²⁴ E. Thomson,⁴⁴ P. Tipton,⁵⁹ V. Tiwari,¹² S. Tkaczyk,¹⁷ D. Toback,⁵² S. Tokar,¹⁴ K. Tollefson,³⁵ T. Tomura,⁵⁴ D. Tonelli,¹⁷ S. Torre,¹⁹ D. Torretta,¹⁷ S. Tourneur,⁴³ W. Trischuk,³³ Y. Tu,⁴⁴ N. Turini,⁴⁵ F. Ukegawa,⁵⁴ S. Uozumi,⁵⁴ S. Vallecorsa,²⁰ N. van Remortel,²³ A. Varganov,³⁴ E. Vataga,³⁶ F. Vázquez,^{l,18} G. Velev,¹⁷ C. Vellidis,^{a,45} V. Veszpremi,⁴⁷ M. Vidal,³¹ R. Vidal,¹⁷ I. Vila,¹¹ R. Vilar,¹¹ T. Vine,³⁰ M. Vogel,³⁶ I. Volobouev,^{q,28} G. Volpi,⁴⁵ F. Würthwein,⁹ P. Wagner,⁴⁴ R.G. Wagner,² R.L. Wagner,¹⁷ J. Wagner-Kuhr,²⁶ W. Wagner,²⁶ T. Wakisaka,⁴⁰ R. Wallny,⁸ S.M. Wang,¹ A. Warburton,³³ D. Waters,³⁰ M. Weinberger,⁵² W.C. Wester III,¹⁷ B. Whitehouse,⁵⁵ D. Whiteson,^{e,44} A.B. Wicklund,² E. Wicklund,¹⁷ G. Williams,³³ H.H. Williams,⁴⁴ P. Wilson,¹⁷ B.L. Winer,³⁸ P. Wittich,^{g,17} S. Wolbers,¹⁷ C. Wolfe,¹³ T. Wright,³⁴ X. Wu,²⁰ S.M. Wynne,²⁹ A. Yagil,⁹ K. Yamamoto,⁴⁰ J. Yamaoka,⁵¹ T. Yamashita,³⁹ C. Yang,⁵⁹ U.K. Yang,^{m,13} Y.C. Yang,²⁷ W.M. Yao,²⁸ G.P. Yeh,¹⁷ J. Yoh,¹⁷ K. Yorita,¹³ T. Yoshida,⁴⁰ G.B. Yu,⁴⁸ I. Yu,²⁷ S.S. Yu,¹⁷ J.C. Yun,¹⁷ L. Zanello,⁵⁰ A. Zanetti,⁵³ I. Zaw,²² X. Zhang,²⁴ Y. Zheng,^{b,8} and S. Zucchelli⁵

(CDF Collaboration*)

¹*Institute of Physics, Academia Sinica, Taipei, Taiwan 11529, Republic of China*

²*Argonne National Laboratory, Argonne, Illinois 60439*

³*Institut de Física d'Altes Energies, Universitat Autònoma de Barcelona, E-08193, Bellaterra (Barcelona), Spain*

⁴*Baylor University, Waco, Texas 76798*

⁵*Istituto Nazionale di Fisica Nucleare, University of Bologna, I-40127 Bologna, Italy*

⁶*Brandeis University, Waltham, Massachusetts 02254*

⁷*University of California, Davis, Davis, California 95616*

⁸*University of California, Los Angeles, Los Angeles, California 90024*

⁹*University of California, San Diego, La Jolla, California 92093*

¹⁰*University of California, Santa Barbara, Santa Barbara, California 93106*

¹¹*Instituto de Física de Cantabria, CSIC-University of Cantabria, 39005 Santander, Spain*

¹²*Carnegie Mellon University, Pittsburgh, PA 15213*

¹³*Enrico Fermi Institute, University of Chicago, Chicago, Illinois 60637*

¹⁴*Comenius University, 842 48 Bratislava, Slovakia; Institute of Experimental Physics, 040 01 Kosice, Slovakia*

¹⁵*Joint Institute for Nuclear Research, RU-141980 Dubna, Russia*

¹⁶*Duke University, Durham, North Carolina 27708*

¹⁷*Fermi National Accelerator Laboratory, Batavia, Illinois 60510*

¹⁸*University of Florida, Gainesville, Florida 32611*

¹⁹*Laboratori Nazionali di Frascati, Istituto Nazionale di Fisica Nucleare, I-00044 Frascati, Italy*

²⁰*University of Geneva, CH-1211 Geneva 4, Switzerland*

²¹*Glasgow University, Glasgow G12 8QQ, United Kingdom*

²²*Harvard University, Cambridge, Massachusetts 02138*

²³*Division of High Energy Physics, Department of Physics,*

University of Helsinki and Helsinki Institute of Physics, FIN-00014, Helsinki, Finland

- ²⁴University of Illinois, Urbana, Illinois 61801
²⁵The Johns Hopkins University, Baltimore, Maryland 21218
²⁶Institut für Experimentelle Kernphysik, Universität Karlsruhe, 76128 Karlsruhe, Germany
²⁷Center for High Energy Physics: Kyungpook National University, Daegu 702-701, Korea; Seoul National University, Seoul 151-742, Korea; Sungkyunkwan University, Suwon 440-746, Korea; Korea Institute of Science and Technology Information, Daejeon, 305-806, Korea; Chonnam National University, Gwangju, 500-757, Korea
²⁸Ernest Orlando Lawrence Berkeley National Laboratory, Berkeley, California 94720
²⁹University of Liverpool, Liverpool L69 7ZE, United Kingdom
³⁰University College London, London WC1E 6BT, United Kingdom
³¹Centro de Investigaciones Energeticas Medioambientales y Tecnologicas, E-28040 Madrid, Spain
³²Massachusetts Institute of Technology, Cambridge, Massachusetts 02139
³³Institute of Particle Physics: McGill University, Montréal, Canada H3A 2T8; and University of Toronto, Toronto, Canada M5S 1A7
³⁴University of Michigan, Ann Arbor, Michigan 48109
³⁵Michigan State University, East Lansing, Michigan 48824
³⁶University of New Mexico, Albuquerque, New Mexico 87131
³⁷Northwestern University, Evanston, Illinois 60208
³⁸The Ohio State University, Columbus, Ohio 43210
³⁹Okayama University, Okayama 700-8530, Japan
⁴⁰Osaka City University, Osaka 588, Japan
⁴¹University of Oxford, Oxford OX1 3RH, United Kingdom
⁴²University of Padova, Istituto Nazionale di Fisica Nucleare, Sezione di Padova-Trento, I-35131 Padova, Italy
⁴³LPNHE, Universite Pierre et Marie Curie/IN2P3-CNRS, UMR7585, Paris, F-75252 France
⁴⁴University of Pennsylvania, Philadelphia, Pennsylvania 19104
⁴⁵Istituto Nazionale di Fisica Nucleare Pisa, Universities of Pisa, Siena and Scuola Normale Superiore, I-56127 Pisa, Italy
⁴⁶University of Pittsburgh, Pittsburgh, Pennsylvania 15260
⁴⁷Purdue University, West Lafayette, Indiana 47907
⁴⁸University of Rochester, Rochester, New York 14627
⁴⁹The Rockefeller University, New York, New York 10021
⁵⁰Istituto Nazionale di Fisica Nucleare, Sezione di Roma 1, University of Rome “La Sapienza,” I-00185 Roma, Italy
⁵¹Rutgers University, Piscataway, New Jersey 08855
⁵²Texas A&M University, College Station, Texas 77843
⁵³Istituto Nazionale di Fisica Nucleare, University of Trieste/ Udine, Italy
⁵⁴University of Tsukuba, Tsukuba, Ibaraki 305, Japan
⁵⁵Tufts University, Medford, Massachusetts 02155
⁵⁶Waseda University, Tokyo 169, Japan
⁵⁷Wayne State University, Detroit, Michigan 48201
⁵⁸University of Wisconsin, Madison, Wisconsin 53706
⁵⁹Yale University, New Haven, Connecticut 06520

(Dated: October 29, 2018)

We measure the time dependence of the ratio of decay rates for the rare decay $D^0 \rightarrow K^+ \pi^-$ to the Cabibbo-favored decay $D^0 \rightarrow K^- \pi^+$. We use a signal of 12.7×10^3 $D^0 \rightarrow K^+ \pi^-$ decays with proper decay times between 0.75 and 10 mean D^0 lifetimes. The data sample was recorded with the CDF II detector at the Fermilab Tevatron and corresponds to an integrated luminosity of 1.5 fb^{-1} for $p\bar{p}$ collisions at $\sqrt{s} = 1.96 \text{ TeV}$. We search for $D^0 - \bar{D}^0$ mixing and measure the mixing parameters to be $R_D = (3.04 \pm 0.55) \times 10^{-3}$, $y' = (8.5 \pm 7.6) \times 10^{-3}$, and $x'^2 = (-0.12 \pm 0.35) \times 10^{-3}$. We report Bayesian probability contours in the $x'^2 - y'$ plane and find that the data are inconsistent with the no-mixing hypothesis with a probability equivalent to 3.8 Gaussian standard deviations.

PACS numbers: 13.20.Fc, 13.25.Ft, 14.40.Lb

*With visitors from ^aUniversity of Athens, 15784 Athens, Greece, ^bChinese Academy of Sciences, Beijing 100864, China, ^cUniversity of Bristol, Bristol BS8 1TL, United Kingdom, ^dUniversity Libre

de Bruxelles, B-1050 Brussels, Belgium, ^eUniversity of California Irvine, Irvine, CA 92697, ^fUniversity of California Santa Cruz, Santa Cruz, CA 95064, ^gCornell University, Ithaca, NY 14853,

Since the discovery of the charm quark in 1974 [1, 2], physicists have been searching for the oscillation of neutral charm mesons between particle and anti-particle states. Such behavior is referred to as “mixing”, as first explained in 1955 [3] for the K^0 meson in terms of quantum-mechanical mixed states. Mixing was next observed for B_d^0 mesons in 1987 [4, 5]. The years 2006 and 2007 have seen landmark new results on mixing: observation of B_s mixing from the CDF experiment [6] and evidence for D^0 mixing from the Belle [7] and BABAR [8] experiments.

The recent evidence for D^0 mixing comes from two different types of measurements. The Belle Collaboration found direct evidence for a longer and shorter lived D^0 meson, in analogy to the well-known case for K^0 mesons. They found significantly different decay time distributions for D^0 decays to the CP-eigenstates K^+K^- and $\pi^+\pi^-$ compared to that for the CP-mixed state $K^-\pi^+$. (In this Letter, reference to a specific decay chain implicitly includes the charge-conjugate decay.) No other experiment has confirmed the evidence for lifetime differences among these decays. The evidence for D^0 mixing found in the BABAR experiment is a difference in decay time distribution for $D^0 \rightarrow K^+\pi^-$ compared to that for the Cabibbo-favored (CF) decay $D^0 \rightarrow K^-\pi^+$. Such a difference depends on the combined effects of differences in the masses and lifetimes of the D^0 meson weak eigenstates. This same measurement was made in the Belle experiment [9], but evidence for mixing was not seen. In this Letter, we present a new measurement of the same D^0 mixing process as used by BABAR for their evidence.

In the standard model, the decay $D^0 \rightarrow K^+\pi^-$ proceeds through a doubly Cabibbo-suppressed (DCS) “tree” diagram, and may also result from a mixing process ($\bar{D}^0 \leftrightarrow D^0$), if it exists, followed by a CF decay ($\bar{D}^0 \rightarrow K^+\pi^-$). The DCS decay rate depends on Cabibbo-Kobayashi-Maskawa quark-mixing matrix elements and on the magnitude of SU(3) flavor symmetry violation [10]. Mixing may occur through two distinct types of second-order weak processes. In the first, the D^0 evolves into a virtual (“long-range”) intermediate state such as $\pi^+\pi^-$, which subsequently evolves to a \bar{D}^0 . The magnitude of the amplitude for long-range mixing has been estimated using strong interaction models [11], but

has not been determined using a QCD calculation from first principles. The second type of second-order weak process is short-range [12], with either a “box” or “penguin” topology. Short-range mixing is negligible in the standard model. However, exotic weakly interacting particles could enhance the short-range mixing and provide a signature of new physics [13, 14, 15].

The ratio R of $D^0 \rightarrow K^+\pi^-$ to $D^0 \rightarrow K^-\pi^+$ decay rates can be approximated [16, 17] as a simple quadratic function of t/τ , where t is the proper decay time and τ is the mean D^0 lifetime. This form is valid assuming CP conservation and small values for the parameters $x = \Delta M/\Gamma$ and $y = \Delta\Gamma/2\Gamma$, where ΔM is the mass difference between the D^0 meson weak eigenstates, $\Delta\Gamma$ is the decay width difference, and Γ is the average decay width of the eigenstates. Under the assumptions stated above,

$$R(t/\tau) = R_D + \sqrt{R_D}y'(t/\tau) + \frac{x'^2 + y'^2}{4}(t/\tau)^2, \quad (1)$$

where R_D is the squared modulus of the ratio of DCS to CF amplitudes. The parameters x' and y' are linear combinations of x and y according to the relations

$$x' = x \cos \delta + y \sin \delta \quad \text{and} \quad y' = -x \sin \delta + y \cos \delta,$$

where δ is the strong interaction phase difference between the DCS and CF amplitudes. In the absence of mixing, $x' = y' = 0$ and $R(t/\tau) = R_D$.

Our measurement uses data collected by the CDF II detector at the Fermilab Tevatron collider, from February 2002 to January 2007, corresponding to an integrated luminosity of $\approx 1.5 \text{ fb}^{-1}$ for $p\bar{p}$ collisions at $\sqrt{s} = 1.96 \text{ TeV}$. CDF II [18] is a multi-purpose detector with a magnetic spectrometer surrounded by a calorimeter and a muon detector. The detector components pertinent to this analysis are the silicon microstrip vertex detector, the multi-wire drift chamber (COT), and the 1.4 T magnet which together measure the trajectories and momenta of charged particles. The COT measures ionization energy loss for a charged particle, which is used for particle identification (PID).

Events are selected in real time with a trigger system developed for a broad class of heavy flavor decays. The trigger requirements used here are the same as those described for our previous measurement of the time-integrated value of R [19], which used a smaller data sample. The trigger selects events with a pair of oppositely charged particles that are consistent with originating from a secondary decay vertex separated from the beamline.

In the off-line analysis, we reconstruct the “right-sign” (RS) CF decay chain $D^{*+} \rightarrow \pi^+D^0$, $D^0 \rightarrow K^-\pi^+$, and the “wrong-sign” (WS) decay chain $D^{*+} \rightarrow \pi^+D^0$, $D^0 \rightarrow K^+\pi^-$. The relative charges of the pions determine whether the decay chain is RS (like charge) or WS (opposite charge). The reconstruction method is similar

^hUniversity of Cyprus, Nicosia CY-1678, Cyprus, ⁱUniversity College Dublin, Dublin 4, Ireland, ^jUniversity of Edinburgh, Edinburgh EH9 3JZ, United Kingdom, ^kUniversity of Heidelberg, D-69120 Heidelberg, Germany, ^lUniversidad Iberoamericana, Mexico D.F., Mexico, ^mUniversity of Manchester, Manchester M13 9PL, England, ⁿNagasaki Institute of Applied Science, Nagasaki, Japan, ^oUniversity de Oviedo, E-33007 Oviedo, Spain, ^pQueen Mary, University of London, London, E1 4NS, England, ^qTexas Tech University, Lubbock, TX 79409, ^rIFIC(CSIC-Universitat de Valencia), 46071 Valencia, Spain.

to that used for our previous time-independent measurement. The RS and WS D^* decays have the same kinematics, and differ only in decay time distributions. To reduce systematic uncertainties, we use the same selection criteria (cuts) for both the RS and WS decay modes. Analysis cuts were optimized before the WS candidates were revealed, and were chosen to maximize the expected WS signal significance.

The D^0 candidate reconstruction starts with a pair of tracks from oppositely charged particles that satisfy the trigger requirements. The tracks are considered with both $K^-\pi^+$ and π^-K^+ interpretations. A third “tagging” track, required to have $p_T \geq 0.3$ GeV/ c , is used to form a D^* candidate when considered as a pion and combined with the D^0 candidate.

We apply two cuts to reduce the background to the WS signal from RS decays where the D^0 decay tracks are misidentified because the kaon and pion assignments are mistakenly interchanged. As determined from the data, 96.4% of D^0 decays with correct mass assignment are reconstructed with $K\pi$ invariant mass $m_{K\pi}$ within 20 MeV/ c^2 of the D^0 mass. The $m_{K\pi}$ distribution for misidentified D^0 decays is much broader, and has only 22% of the events within the same mass range. We remove WS candidates that have a RS mass within that range. This cut excludes 96.4% of RS decays and retains 78% of the WS signal. We also impose a cut based on PID which is used to distinguish pions from kaons for all three tracks in the decay chain. This cut, described in Ref. [19], further helps to reject misidentified decays.

We use a series of cuts based on the decay topology of signal events in which a D^* is produced at the primary vertex, the tagging pion also originates from the primary vertex, and the D^0 travels a measurable distance before decay. The vertex-based cuts reduce combinatoric background from improper combinations involving one or more tracks that do not originate from the D^* decay chain of interest. We require the transverse decay length significance L_{xy}/σ_{xy} to be greater than 4, where $L_{xy} = \vec{r} \cdot \vec{p}_T/p_T$, \vec{r} is the distance between the primary and D^0 decay vertices, \vec{p}_T is the transverse component of the momentum of the D^0 candidate with respect to the beamline, and σ_{xy} is the uncertainty on L_{xy} . The tagging pion track must have $d_0 < 500$ μm , where the transverse impact parameter d_0 is the distance of closest approach between a track and the primary vertex in the plane transverse to the beamline. The tagging pion must also have a point of closest approach to the primary vertex less than 1.5 cm along the beamline.

The ratio t/τ is determined for each D^0 candidate by $t/\tau = m_{D^0} L_{xy}/(p_T \tau)$, where $m_{D^0} = 1.8648$ GeV/ c^2 and $\tau = 410.1$ fs are the world average values for the D^0 invariant mass and lifetime, respectively [20]. To study $R(t/\tau)$, we divide the data into 20 bins of t/τ ranging from 0.75 to 10.0, choosing bins of increasing size from 0.25 to 2.0 to reduce statistical uncertainty at larger

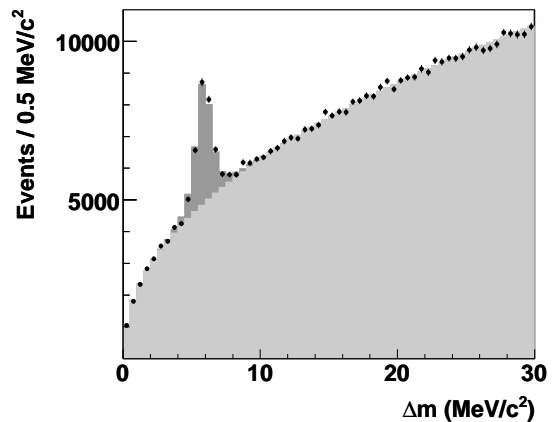


FIG. 1: Time-integrated distribution for “wrong-sign” $D^0 \rightarrow K^+\pi^-$ signal yield as a function of Δm . Also shown is the result of a least-squares fit using an empirical function for the signal (dark shaded region) and a power law for the background (light shaded region).

times. The bin sizes are larger than the t/τ resolution of ≈ 0.16 .

After RS and WS candidates are separately divided into t/τ bins, they are further divided into bins of mass difference $\Delta m \equiv m_{K\pi\pi} - m_{K\pi} - m_\pi$. For each Δm bin, we perform a binned maximum likelihood fit of the corresponding $m_{K\pi}$ distribution to determine the D^0 signal yield. The distribution of D^0 signal yield versus Δm is fit using a least-squares method to get the D^* signal for each time bin. The D^* fit procedure is illustrated by the time-integrated WS Δm distribution shown in Fig. 1.

The signal shapes for the individual $m_{K\pi}$ and Δm distributions are fixed from the RS time-integrated fits. For each $m_{K\pi}$ distribution, a parabola with floating parameters is used to fit the background. The background shapes for all the Δm WS (RS) distributions are fixed to the shape determined for the time-integrated WS (RS) distribution. The amplitudes of the signal and background shapes are determined independently for all $m_{K\pi}$ and Δm fits. The RS distributions have similar amounts of background as the WS distributions, but the RS signal is about 250 times larger.

The D^* mesons that originate from beauty hadron (B) decays must be treated as background to avoid the complication of measuring the D^0 decay length from the B decay point instead of the primary vertex. The D^* mesons produced promptly at the primary vertex have a narrow d_0 distribution, with a shape independent of t/τ . The background from non-prompt D^* mesons from the decay chain $B \rightarrow D^* \rightarrow D^0$ have a broad d_0 distribution, due to the decay length of the B hadrons. The width of the broad distribution increases with increasing t/τ . An example d_0 distribution is shown in Fig. 2. The shapes of the prompt and broad distributions are determined from RS data. The WS shapes are the same as

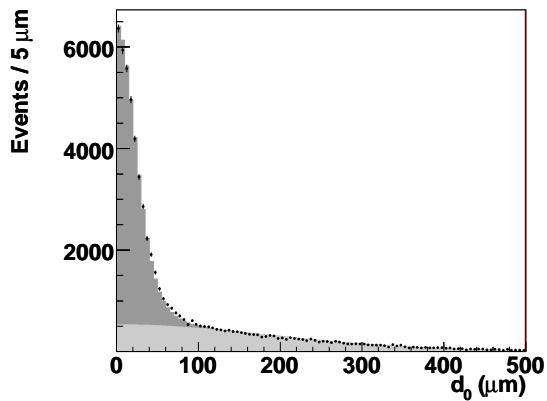


FIG. 2: The distribution of transverse impact parameter d_0 for $5 < t/\tau < 6$ for “right sign” background-subtracted D^* mesons. The result of a binned maximum likelihood fit shows the narrow peak due to promptly produced D^* mesons (dark shaded) and the broad distribution due to non-prompt D^* mesons from B decay (light shaded).

the RS shapes. For each of the 20 t/τ bins, the prompt WS (RS) signal is determined from the number of WS (RS) D^* mesons and the shapes of the d_0 distributions. The ratio of non-prompt to prompt signal is ≈ 0.02 at $t/\tau = 2$ and increases with increasing t/τ due to the faster exponential fall-off with t/τ for D^0 compared to B . At $t/\tau = 7$, the ratio is ≈ 1 .

The time-integrated prompt D^* signals are $(12.7 \pm 0.3) \times 10^3$ WS events and $(3.044 \pm 0.002) \times 10^6$ RS events. The ratios of prompt WS to RS signal for the 20 t/τ bins are shown in Fig. 3. The uncertainties for each bin include statistical and systematic contributions. The significant systematic uncertainties are due to the background shapes for the $m_{K\pi}$, Δm , and d_0 distributions, which are described by parameters that are allowed to vary in the fitting procedure. We used simulation to confirm that our choice of decay time bins does not systematically affect the result. The detector acceptances for RS and WS decays are nearly identical, and their difference contributes a negligible systematic uncertainty in the ratio R . The large uncertainty in the first t/τ bin is due to low signal statistics caused by the trigger turn-on at small t/τ . In the last two bins, the uncertainties are large because the exponential fall-off of the WS signal with t/τ results in smaller numbers of signal events.

A least-squares parabolic fit of the data in Fig. 3 to Eq. (1) determines the values and uncertainties for the parameters R_D , y' , and x'^2 , which are listed in Table I. Since the value of x'^2 is unphysical (less than zero), but consistent with zero, we also fit the data with the constraint $x'^2 = 0$. The values of R_D and y' are consistent with and without the constraint. The values and precision of the parameters measured by CDF are comparable to those from the best previous measurements, as shown

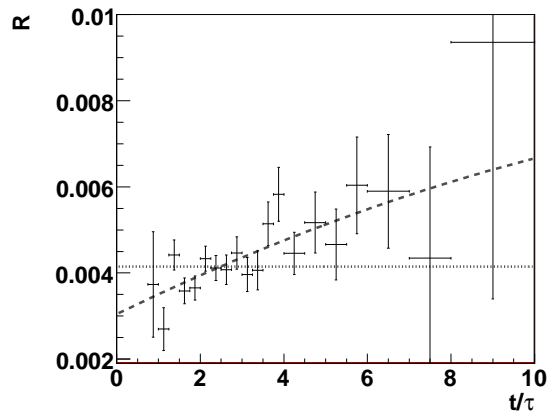


FIG. 3: Ratio of prompt D^* “wrong-sign” to “right sign” decays as a function of normalized proper decay time. The dashed curve is from a least-squares parabolic fit, which determines the parameters R_D , y' , and x'^2 . The dotted line is the fit assuming no mixing.

TABLE I: Fit results for the $R(t/\tau)$ distribution. The uncertainties include statistical and systematic components. The correlation coefficient between y' and x'^2 for the unconstrained fit is -0.98 . The no-mixing fit is consistent with our previous time-independent result [19].

Fit type	$R_D(10^{-3})$	$y'(10^{-3})$	$x'^2(10^{-3})$	$\chi^2 / \text{d.o.f.}$
Unconstrained	3.04 ± 0.55	8.5 ± 7.6	-0.12 ± 0.35	19.2 / 17
Physically allowed	3.22 ± 0.23	6.0 ± 1.4	0	19.3 / 18
No mixing	4.15 ± 0.10	0	0	36.8 / 19

in Table II.

To determine the consistency of our data with the no-mixing hypothesis, we compute Bayesian contours containing the region with the highest posterior probability. The probability density is calculated as the product of a likelihood \mathcal{L} and a prior, divided by a normalization factor. The likelihood is $\mathcal{L} = \exp(-\chi^2/2)$, where χ^2 is

TABLE II: Comparison of the CDF result with recent measurements. All results use $D^0 \rightarrow K^+\pi^-$ decays and fits assuming no CP violation. The uncertainties include statistical and systematic components. The significance for no mixing is given in terms of the equivalent number of Gaussian standard deviations.

Experiment	$R_D(10^{-3})$	$y'(10^{-3})$	$x'^2(10^{-3})$	Mixing
				Signif.
CDF	3.04 ± 0.55	8.5 ± 7.6	-0.12 ± 0.35	3.8
BABAR [8]	3.03 ± 0.19	9.7 ± 5.4	-0.22 ± 0.37	3.9
Belle [9]	3.64 ± 0.17	$0.6^{+4.0}_{-3.9}$	$0.18^{+0.21}_{-0.23}$	2.0

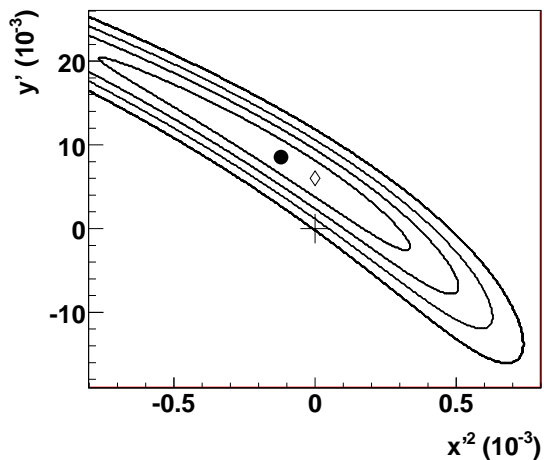


FIG. 4: Bayesian probability contours in the $x'^2 - y'$ parameter space corresponding to one through four equivalent Gaussian standard deviations. The closed circle shows the unconstrained fit values for the mixing parameters. The open diamond shows the values from the physically allowed fit ($x'^2 \geq 0$). The cross shows the no-mixing point.

computed from the data in Fig. 3 for a particular set of fit parameters. The normalization factor is the integral of \mathcal{L} over the parameter space. A flat prior is used for all three parameters, and R_D is treated as a Bayesian nuisance parameter. The contours are insensitive to modest changes in the prior. The contours in the $x'^2 - y'$ plane are shown in Fig. 4. The no-mixing point lies on the contour which excludes a region containing a probability of 1.5×10^{-4} , equivalent to 3.8 Gaussian standard deviations. We also computed contours with the constraint $x'^2 \geq 0$ and find a probability for no-mixing consistent with the value obtained without the constraint.

We tried alternate procedures to determine the probability for no mixing. We fit the data in Fig. 3 with the constraint $y' = x'^2 = 0$, with results as given in Table I. The change in log likelihood ($-2\Delta \ln \mathcal{L}$) between the unconstrained and no-mixing fits has an approximately chi-square distribution for two degrees of freedom. From Table I, $-2\Delta \ln \mathcal{L} = 17.6$, which corresponds to a probability of 1.6×10^{-4} . We also made a frequentist check using ensembles of simulated $R(t/\tau)$ measurements without mixing. The probability for a simulation to have a value of $-2\Delta \ln \mathcal{L} \geq 17.6$ is 1.3×10^{-4} . The probabilities from both of these checks are consistent with that obtained using Bayesian contours.

In conclusion, our data shows evidence for $D^0 - \bar{D}^0$ mixing in the $K^+\pi^-$ channel, providing the first confirmation of the evidence from the *BABAR* experiment. The mixing could be due to standard model long-range intermediate states or due to new physics. Improved reliability of standard model calculations and future measurements of mixing signatures with improved precision

are needed to explain this phenomenon.

We thank the Fermilab staff and the technical staffs of the participating institutions for their vital contributions. This work was supported by the U.S. Department of Energy and National Science Foundation; the Italian Istituto Nazionale di Fisica Nucleare; the Ministry of Education, Culture, Sports, Science and Technology of Japan; the Natural Sciences and Engineering Research Council of Canada; the National Science Council of the Republic of China; the Swiss National Science Foundation; the A.P. Sloan Foundation; the Bundesministerium für Bildung und Forschung, Germany; the Korean Science and Engineering Foundation and the Korean Research Foundation; the Science and Technology Facilities Council and the Royal Society, UK; the Institut National de Physique Nucleaire et Physique des Particules/CNRS; the Russian Foundation for Basic Research; the Comisión Interministerial de Ciencia y Tecnología, Spain; the European Community's Human Potential Programme; the Slovak R&D Agency; and the Academy of Finland.

-
- [1] J.J. Aubert *et al.*, Phys. Rev. Lett. **33**, 1404 (1974).
 - [2] J.E. Augustin *et al.*, Phys. Rev. Lett. **33**, 1406 (1974).
 - [3] M. Gell-Mann and A. Pais, Phys. Rev. **97**, 1387 (1955).
 - [4] C. Albajar *et al.* (UA1 Collaboration), Phys. Lett. B **186**, 247 (1987).
 - [5] H. Albrecht *et al.* (ARGUS Collaboration), Phys. Lett. B **192**, 245 (1987).
 - [6] A. Abulencia *et al.* (CDF Collaboration), Phys. Rev. Lett. **97**, 242003 (2006).
 - [7] M. Starič *et al.* (Belle Collaboration), Phys. Rev. Lett. **98**, 211803 (2007).
 - [8] B. Aubert *et al.* (*BABAR* Collaboration), Phys. Rev. Lett. **98**, 211802 (2007).
 - [9] L. M. Zhang *et al.* (Belle Collaboration), Phys. Rev. Lett. **96**, 151801 (2006).
 - [10] M. Gronau and J. L. Rosner, Phys. Lett. B **500**, 247 (2001).
 - [11] A. F. Falk *et al.*, Phys. Rev. D **69**, 114021 (2004).
 - [12] E. Golowich and A. A. Petrov, Phys. Lett. B **625**, 53 (2005).
 - [13] G. Burdman and I. Shipsey, Annu. Rev. Nucl. Sci. **53**, 431 (2003). See section 2.3.
 - [14] E. Golowich, S. Pakvasa and A. A. Petrov, Phys. Rev. Lett. **98**, 181801 (2007).
 - [15] E. Golowich, J. Hewett, S. Pakvasa, and A. A. Petrov, arXiv:0705.3650, to appear in Phys. Rev. D.
 - [16] G. Blaylock *et al.*, Phys. Lett. B **355**, 555 (1995).
 - [17] R. Godang *et al.* (CLEO Collaboration), Phys. Rev. Lett. **84**, 5038 (2000).
 - [18] D. Acosta *et al.* (CDF Collaboration), Phys. Rev. D **71**, 032001 (2005).
 - [19] A. Abulencia *et al.* (CDF Collaboration), Phys. Rev. D **74**, 031109(R) (2006).
 - [20] W.-M. Yao *et al.* (Particle Data Group), J. Phys. G **33**, 1 (2006).